Oxytocin regulation of social transmission of fear in zebrafish reveals its evolutionary conserved role in emotional contagion

Ibukun Akinrinade[1, 2, &], Kyriacos Kareklas[1,&], Magda Teles[1], Thais K. Reis[1], Michael Gliksberg[3], Giovanni Petri[4], Gil Levkowitz[3,5], Rui F. Oliveira [1,6,7,*]

[1] Integrative Behavioural Biology Lab, Instituto Gulbenkian de Ciência, Oeiras 2780-156, Portugal

[2] Department of Physiology and Phramacology, Cumming School of Medicine, University of Calgary; 2500 University Drive NW, Calgary Alberta T2N 1N4, Canada

[3] Department of Molecular Cell Biology, Weizmann Institute of Science, Rehovot 7610001, Israel

[4] ISI Foundation and ISI Global Science Foundation, Torino 10126, Italy

[5] Department of Molecular Neuroscience, Weizmann Institute of Science, Rehovot 7610001, Israel

[6] ISPA-Instituto Universitário, Lisboa 1149-041, Portugal

[7] Champalimaud Neuroscience Program, Champalimaud Centre for the Unknown, Lisbon 1400-038, Portugal

[&] indicates joint first authorship with first authors listed by alphabetical order.

* corresponding author: ruiol@ispa.pt

Abstract: Emotional contagion is the most ancestral form of empathy that relies on simple perception-action mechanisms, on top of which more complex forms of empathic behaviors, such as consolation and helping, have evolved. Here we tested to what extent the proximate mechanisms of emotional contagion are evolutionary conserved by assessing the role of oxytocin, known to regulate empathic behaviors in mammals, in social fear contagion in zebrafish, which represents an evolutionary divergent line to that of tetrapods, within vertebrates. Using mutants for the ligand of the fish oxytocin nonapeptide and both of its receptors in zebrafish we showed that oxytocin is necessary for observer zebrafish to copy the distressed behavior of conspecific demonstrators. Exogeneous administration of oxytocin to the ligand mutant rescued the ability of observers to express social fear transmission, indicating that oxytocin is not only necessary but also sufficient for emotional contagion. The brain regions in the ventral telencephalon that are associated with emotional contagion in zebrafish are homologous to those involved in the same process in rodents (e.g. striatum, lateral septum), exhibiting similar inhibitory and excitatory controls, and receiving direct projections from oxytocinergic neurons located in the pre-optic area. Finally, we ruled out the hypothesis that social transmission of fear in zebrafish merely relies on behavior contagion by motor imitation, and we showed that it rather relies on emotion recognition. Together, our results support an evolutionary conserved role for oxytocin as a key regulator of basic empathic behaviors across vertebrates.

One-Sentence Summary: Oxytocin is necessary and sufficient for social fear contagion in zebrafish supporting an evolutionary conserved role for oxytocin in emotional contagion among vertebrates.

Main Text

Emotional contagion, described as the ability to match the emotional state of another individual, has been considered the most ancestral form of empathy, on top of which more complex forms of empathic behaviors, such as consolation and helping, have evolved in species endowed with more complex cognitive abilities (e.g. rodents, elephants, dolphins, primates [1-3]). Emotional contagion relies on simple perception-action mechanisms and provides important adaptive advantages to social living species [1]. It enhances social cohesion and the establishment of social bonds, and promotes the rapid spread of fear among group members once a threat is detected (e.g. predators), which allows individuals to survive potential dangers without directly experiencing them [3]. Therefore, emotional contagion is expected to be phylogenetically ancient, being present even in species with less elaborate social cognition. Indeed, social contagion of fear has been recently described in zebrafish (*Danio rerio*), consisting the transmission of distress behavior to observers and increases in observer cortisol levels similar to those of target individuals [4-6]. Moreover, behavioral responses are influenced by familiarity, with familiar distressed target fish eliciting stronger distress responses in observers [5]. The face validity of this transmission of distress behavior as emotional contagion can also be argued by comparison with mammalian models of emotional contagion, such as facial expressions in orangutans [7] and freezing in rodents [8]. However, to what extent the social contagion of fear observed in fish and in mammals is homologous, or represents a case of convergent evolution, remains an open question. To disentangle these two hypotheses, we investigated if emotional contagion in zebrafish shares the same proximate mechanisms that have been described for mammals. We focused on the oxytocin signaling system since nonapeptides of the oxytocin family are evolutionarily conserved across vertebrates [9] and have been implicated in the regulation of emotional contagion in rodents [10, 11] and fear recognition in humans [12, 13].

Here we have used zebrafish mutant lines for the ligand (*oxt*) and the two receptors (*oxtr* and *oxtrl*) of the zebrafish oxytocin nonapeptide (CYISNCPIG-NH_2, aka isotocin [9]) to assess the role of oxytocin in fear contagion. In zebrafish, injured individuals release an alarm substance from their skin into the water, which is detected through olfaction eliciting a distress response consisting of erratic movement followed by freezing behavior [14]. The sight of conspecifics in distress also elicits the expression of this response in observers, indicating the occurrence of fear contagion in zebrafish [4-6] (Fig. 1). Therefore, we have used an experimental paradigm in which a naïve observer fish watches a conspecific shoal in a neighboring tank (i.e. without chemical communication), to which we have administered either water (control) or the alarm substance (Fig. 1A). Given that freezing behavior was a more consistent distress response in wild types than erratic movement (Fig. 1B-K), we have used it as a read-out for fear contagion. Observer individuals of all wild type control lines (i.e. $oxt^{+/+}$, $oxtr^{+/+}$ and $oxtrl^{+/+}$) significantly increased their freezing behavior when exposed to a distressed shoal. In contrast, observer individuals of all the mutant lines (i.e. $oxt^{-/-}$, $oxtr^{-/-}$ and $oxtrl^{-/-}$) failed to significantly increase their freezing behavior when exposed to a distressed shoal (Fig. 1C, E, G). This indicates that oxytocin signaling is necessary for fear contagion in zebrafish. Moreover, we have administered exogenous oxytocin to the ligand mutants and their controls to assess if it could recue the fear contagion phenotype. We have also injected another group

of ligand mutants and their respective control with the vehicle solution to control for putative stressful effects of the injection. Mutants injected with oxytocin also increased significantly their freezing behavior when exposed to distressed conspecifics, indicating that oxytocin is both necessary and sufficient for emotional contagion (Fig. 1E, G).

To characterize the neural circuits associated with emotional contagion in zebrafish we examined the expression of a neuronal activity marker, phospho-S6 ribosomal protein (pS6), in a set of forebrain and midbrain areas involved in social decision-making across vertebrates (i.e. social decision-making network [15]). Significant changes were identified in two of these areas, the ventral (Vv) and central nucleus (Vc) of the ventral telencephalic area (Fig. 2A). The Vv is a putative homologue of the mammalian lateral septum and the Vc of the mammalian striatum. Remarkably, the expression, recognition and sharing of emotions in humans also relies on the regulation of activity in these forebrain areas by oxytocin, even if higher order empathic functions are dependent on neocortical circuits [16-19]. In zebrafish, we find that both areas exhibit a decrease in activity associated with the expression of freezing behavior in observer wild-types and an increase in activity with the lack of response in *oxtr* mutants (Fig. 2B). This suggests that zebrafish distress behavior during contagion is mediated by decreases in inhibitory cell activity and that overactivation of these cells in mutants prevents the expression of this behavior. To test this, we used a double reporter line for both excitatory (glutamate: *vglut2/dsRed*) and inhibitory (γ-aminobutyric acid, GABA: *gad1b/GFP*) neurotransmission (Fig. 2C). Compared to controls, during contagion the Vv indeed exhibits greater activity in inhibitory cells ($\chi^2_{1,13} = 5.09$, $p = 0.024$), but the Vc instead exhibits increased activity in excitatory cells ($\chi^2_{1,13} = 9.90$, $p = 0.002$). Notably, the oxytocinergic modulation of GABAergic inhibition is also exhibited in the lateral septum of mice during social fear transmission [17]. The zebrafish Vv conserves the role of the mammalian lateral septum as a functional connectivity area between the social behavior and mesolimbic system [15]. Thus, the decreasing inhibition when distress is observed, enables otherwise suppressed signals during control conditions to be relayed between areas of the network. In contrast, the Vc conserves the role of the striatum as part of the mesolimbic reward pathway for downstream other-oriented motor and motivational controls [16, 18], which explain the excitatory increases similar to those noted in parts of the striatum in mice [19]. Because the proportion of active cells during contagion that were either inhibitory or excitatory was a minority (Vc: 31.26%; Vv: 15.86%), the overall decreased activity may relate to other oxytocin induced changes in local cells, likely from shifts in connectivity across the network. Oxytocin regulation of these ventral forebrain areas relies on projections from oxytocin neurons in the pre-optic area (Fig. 2D), and is confirmed by the expression of both zebrafish oxytocin receptors in these areas (*oxtr*, *oxtrl*; Fig S1). Interestingly, both receptors are also expressed across most nodes of the social decision-making network, but the expression of the primary receptor (*oxtr*) is distinctly greater and more widespread (Fig. S1). Thus, we examined the effect of *oxtr* expression on patterns of functional connectivity across the social decision-making network.

In order to study functional connectivity, we constructed networks representing co-activation patterns during contagion and control treatments, for both wild-types and *oxtr* mutants, with positive and negative correlations between nodes indicating excitatory and inhibitory patterns respectively. Although functional distributions differ between wild-types

and mutants under both control and treatment conditions, average inhibition and excitation notably differ only under the fear contagion treatment (Fig. 3). Overall, the absence of emotional contagion in *oxtr* mutants was paralleled by a segregated pattern of functional connectivity (excitatory: $KS = 0.38$, $p < 10^{-6}$; inhibitory: $KS = 0.50$, $p < 10^{-4}$) with significantly greater average excitation in their brain network ($U = 5680$, $p < 10^{-6}$, Cohen's $d = 0.49$) than wild types displaying the socially transmitted distress behavior. In line with our findings in the reporter line, the Vv of wild-types loses all its inhibitory connectivity during treatment, compared to control, but in mutants inhibitory connectivity is partly kept, namely to the anterior tuberal nucleus (ATN). In contrast, the Vc of wild types maintains inhibitory connectivity during contagion, shifting only in target nodes and reducing strong neighboring connections (VD), which may explain the overall reduced activity. We also confirm it exhibits excitatory links, most of which are to non-neighboring nodes and which do not appear in *oxtr* mutants. These include the habenula (HAV), the lateral hypothalamic nucleus (LH), and the posterior dorsal telencephalic area (Dp), which are involved in fear and alarm response [6, 20]. Node centrality also radically shifted in ranking between the brain networks of wild types and *oxtr* mutants, and with fear contagion compared to control (Fig. S2; Table S1). In turn, only a single conserved submodule (at $z > 3$, $p < 0.01$) was shared between wild types and *oxtr* mutants under the fear contagion treatment, and it comprises the dorsal (HAD) and ventral habenula (HAV), the posterior pre-optic area (PPp) and the magnocellular preoptic nucleus (PM). Considering the implication of the habenular nuclei in zebrafish fear responses, and that the pre-optic area responds to the alarm substance [6, 20], this submodule is likely involved in processing fear stimulation in both groups. Interestingly, while the submodule is isolated in *oxtr* mutants, in wild types it is integrated in a larger module together with ventral and dorsal areas of the telencephalon (D, DL, VS), and the ventral zone of the periventricular nucleus (HV). This indicates that oxytocin drives greater functional integration when animals are exposed to distressed conspecifics.

The observed social transmission of fear in zebrafish can be regarded simply as behavior contagion based on motor imitation, or as emotional contagion, which requires the recognition of the demonstrator's state (i.e. emotion) and which triggers an automatic representation of the same state in the observer, causing an equivalent expression of behavior [21]. Although zebrafish match both the behavior and cortisol levels of distressed others [4], this may be either due to recognizing and sharing the internal state of others or because the behavior of others signals local danger (e.g. predators [14]), which triggers proportional physiological and behavioral changes. Therefore, we decided to test state recognition explicitly. To this end, observers of *oxt*, *oxtr* and *oxtrl* mutants and their respective wild-type controls were first exposed to two simultaneous pre-recorded video playbacks of the same demonstrator in conflicting states, neutral (swimming) and periodic distress (three bouts of erratic and freezing repertoire). Then observers were exposed to two videos both showing the demonstrator in the neutral state, where recognition was tested via local preferences based on the previously observed conflicting states (Fig. 4A). During observation, fish oriented towards erratic movement and freezing, thus attention shifted to the distressed behavior and not the level of movement (Fig. S3). Notably, orientation preferences were not different between any of the oxytocin mutants and wild type controls (Fig. 4B – E). In contrast, where wild types

replicate the distress behavior of the demonstrators, oxytocin mutants failed to do so, but the administration of oxytocin to the ligand mutant (*oxt*) rescues the distress contagion (Fig. 4F-I; Fig. S4). This replicated the results of the live demonstrator experiment regarding the necessary and sufficient role of oxytocin and further shows that attention is not moderating these effects. Interestingly, during the test phase, wild type observers were motivated to approach and prefer being near the previously distressed demonstrator, whereas oxytocin mutants do not express a motivation to approach the previously distressed demonstrator (Fig. 4 J-M) and prefer being near the demonstrator that remained in a neutral state (Fig. 4 N-Q). This indicates that oxytocin is necessary and sufficient for zebrafish to recognize the distressed from the neutral behavior in the same conspecific, suggesting the occurrence of an oxytocin-dependent emotion recognition in zebrafish [22, 23]. This is in line with responses in humans and mammals that implicate the recognition of a fearful state in others and not simply their behavior [24, 25]. Moreover, because distressed behavior in zebrafish signals local predation risk [14], our findings also show that oxytocin promotes interaction with distressed others despite heightened local risk. Such other-oriented acts that involve individual costs and benefits for others are typically referred to as prosociality, which is well-defined in mammals where it is also regulated by oxytocin [2, 20 - 22]. In this case the benefit for the receiver can be due to the buffering of distress in the presence of others, which has been also described in zebrafish [20]. Thus, approaching and interacting with a distressed individual may prove to be a prosocial behavior in zebrafish, but further evidence is needed.

The oxytocin regulation of fear contagion in zebrafish described here supports its evolutionary conserved role in emotional contagion, given its similar effects in mammals, where exogeneous administration of oxytocin increases observational fear responses [10, 11]. Furthermore, both in zebrafish and in rodents oxytocin also regulates emotion recognition [24, 26], which is the cognitive basis for emotion contagion. Therefore, it is plausible that oxytocin has been recruited early in the evolution of nonapeptides to regulate ancestral empathic behaviors in group living species, and that it has been evolutionarily co-opted to regulate more complex empathic behaviors, such as consolation and helping [25, 27-30], in species with more complex cognitive abilities. From a translational research perspective our results provide content and construct validity to a phylogenetically distant model of emotional contagion.

References

1. De Waal, F. B. (2008). Putting the altruism back into altruism: the evolution of empathy. *Annual. Reviews of Psychology*, *59*, 279-300.
2. De Waal, F. B., & Preston, S. D. (2017). Mammalian empathy: behavioural manifestations and neural basis. *Nature Reviews Neuroscience*, *18*(8), 498-509.
3. Pérez-Manrique, A., & Gomila, A. (2021). Emotional contagion in nonhuman animals: A review. *Wiley Interdisciplinary Reviews: Cognitive Science*, e1560.
4. Oliveira, R. F., & Faustino, A. I. (2017). Social information use in threat perception: Social buffering, contagion and facilitation of alarm responses. *Communicative & Integrative Biology*, *10*(3), 44329.
5. Silva, P. F., de Leaniz, C. G., & Luchiari, A. C. (2019). Fear contagion in zebrafish: a behaviour affected by familiarity. *Animal Behaviour*, *153*, 95-103.
6. Pinho, J. S., Castilho, M., Sollari, J. S., & Oliveira, R. F. (2020). Innate chemical, but not visual, threat cues have been co-opted as unconditioned stimulus for social fear learning in zebrafish. *Genes, Brain and Behavior*, *19*(8), e12688.

7. Davila Ross, M., Menzler, S., & Zimmermann, E. (2008). Rapid facial mimicry in orangutan play. *Biology letters*, *4*(1), 27-30.
8. Hernandez-Lallement, J., Gómez-Sotres, P., & Carrillo, M. (2020). Towards a unified theory of emotional contagion in rodents—A meta-analysis. *Neuroscience & Biobehavioral Reviews*.
9. Theofanopoulou, C., Gedman, G., Cahill, J. A., Boeckx, C., & Jarvis, E. D. (2021). Universal nomenclature for oxytocin–vasotocin ligand and receptor families. *Nature*, *592*(7856), 747-755.
10. Zoratto, F., Sbriccoli, M., Martinelli, A., Glennon, J. C., Macrì, S., & Laviola, G. (2018). Intranasal oxytocin administration promotes emotional contagion and reduces aggression in a mouse model of callousness. Neuropharmacology, 143, 250-267
11. Pisansky, M. T., Hanson, L. R., Gottesman, I. I., & Gewirtz, J. C. (2017). Oxytocin enhances observational fear in mice. Nature communications, 8(1), 1-11.
12. Zink, C. F., & Meyer-Lindenberg, A. (2012). Human neuroimaging of oxytocin and vasopressin in social cognition. *Hormones and behavior*, *61*(3), 400-409.
13. Shahrestani, S., Kemp, A. H., & Guastella, A. J. (2013). The impact of a single administration of intranasal oxytocin on the recognition of basic emotions in humans: a meta-analysis. *Neuropsychopharmacology*, *38*(10), 1929-1936
14. Speedie, N., & Gerlai, R. (2008). Alarm substance induced behavioral responses in zebrafish (Danio rerio). *Behavioural brain research*, *188*(1), 168-177.
15. O'Connell, L. A., & Hofmann, H. A. (2012). Evolution of a vertebrate social decision-making network. *Science*, *336*(6085), 1154-1157.
16. Lamm, C., Rütgen, M., & Wagner, I. C. (2019). Imaging empathy and prosocial emotions. Neuroscience letters, 693, 49-53.
17. Menon, R., Grund, T., Zoicas, I., Althammer, F., Fiedler, D., Biermeier, V., ... & Neumann, I. D. (2018). Oxytocin signaling in the lateral septum prevents social fear during lactation. Current Biology, 28(7), 1066-1078.
18. Lieberz, J., Scheele, D., Spengler, F. B., Matheisen, T., Schneider, L., Stoffel-Wagner, B., ... & Hurlemann, R. (2020). Kinetics of oxytocin effects on amygdala and striatal reactivity vary between women and men. Neuropsychopharmacology, 45(7), 1134-1140.
19. Moaddab, M., Hyland, B. I., & Brown, C. H. (2015). Oxytocin excites nucleus accumbens shell neurons in vivo. *Molecular and Cellular Neuroscience*, *68*, 323-330.
20. Faustino, A. I., Tacão-Monteiro, A., & Oliveira, R. F. (2017). Mechanisms of social buffering of fear in zebrafish. *Scientific reports*, *7*(1), 1-10.
21. Preston, S. D., & De Waal, F. B. (2002). Empathy: Its ultimate and proximate bases. *Behavioral and brain sciences*, *25*(1), 1-20.
22. Ferretti, V., & Papaleo, F. (2019). Understanding others: emotion recognition in humans and other animals. *Genes, Brain and Behavior*, *18*(1), e12544
23. Nieuwburg, E. G., Ploeger, A., & Kret, M. E. (2021). Emotion recognition in nonhuman primates: How experimental research can contribute to a better understanding of underlying mechanisms. *Neuroscience & Biobehavioral Reviews*, 123, 21-47
24. Ferretti, V., Maltese, F., Contarini, G., Nigro, M., Bonavia, A., Huang, H., ... & Papaleo, F. (2019). Oxytocin signaling in the central amygdala modulates emotion discrimination in mice. *Current Biology*, *29*(12), 1938-1953.
25. Burkett, J. P., Andari, E., Johnson, Z. V., Curry, D. C., de Waal, F. B., & Young, L. J. (2016). Oxytocin-dependent consolation behavior in rodents. *Science*, *351*(6271), 375-378.
26. Rogers-Carter, M. M., Varela, J. A., Gribbons, K. B., Pierce, A. F., McGoey, M. T., Ritchey, M., & Christianson, J. P. (2018). Insular cortex mediates approach and avoidance responses to social affective stimuli. *Nature neuroscience*, *21*(3), 404-414.
27. Li, L. F., Yuan, W., He, Z. X., Wang, L. M., Jing, X. Y., Zhang, J., ... & Tai, F. D. (2019). Involvement of oxytocin and GABA in consolation behavior elicited by socially defeated individuals in mandarin voles. *Psychoneuroendocrinology*, *103*, 14-24.
28. Yamagishi, A., Lee, J., & Sato, N. (2020). Oxytocin in the anterior cingulate cortex is involved in helping behaviour. *Behavioural Brain Research*, *393*, 112790.
29. Kitano, K., Yamagishi, A., Horie, K., Nishimori, K., & Sato, N. (2020). Helping behavior in prairie voles: a model of empathy and the importance of oxytocin. *BioRxiv*. DOI: 10.1101/ 2020.10.20.347872
30. Chang, S. W., Barter, J. W., Ebitz, R. B., Watson, K. K., & Platt, M. L. (2012). Inhaled oxytocin amplifies both vicarious reinforcement and self reinforcement in rhesus macaques (Macaca mulatta). *Proceedings of the National Academy of Sciences*, *109*(3), 959-964.

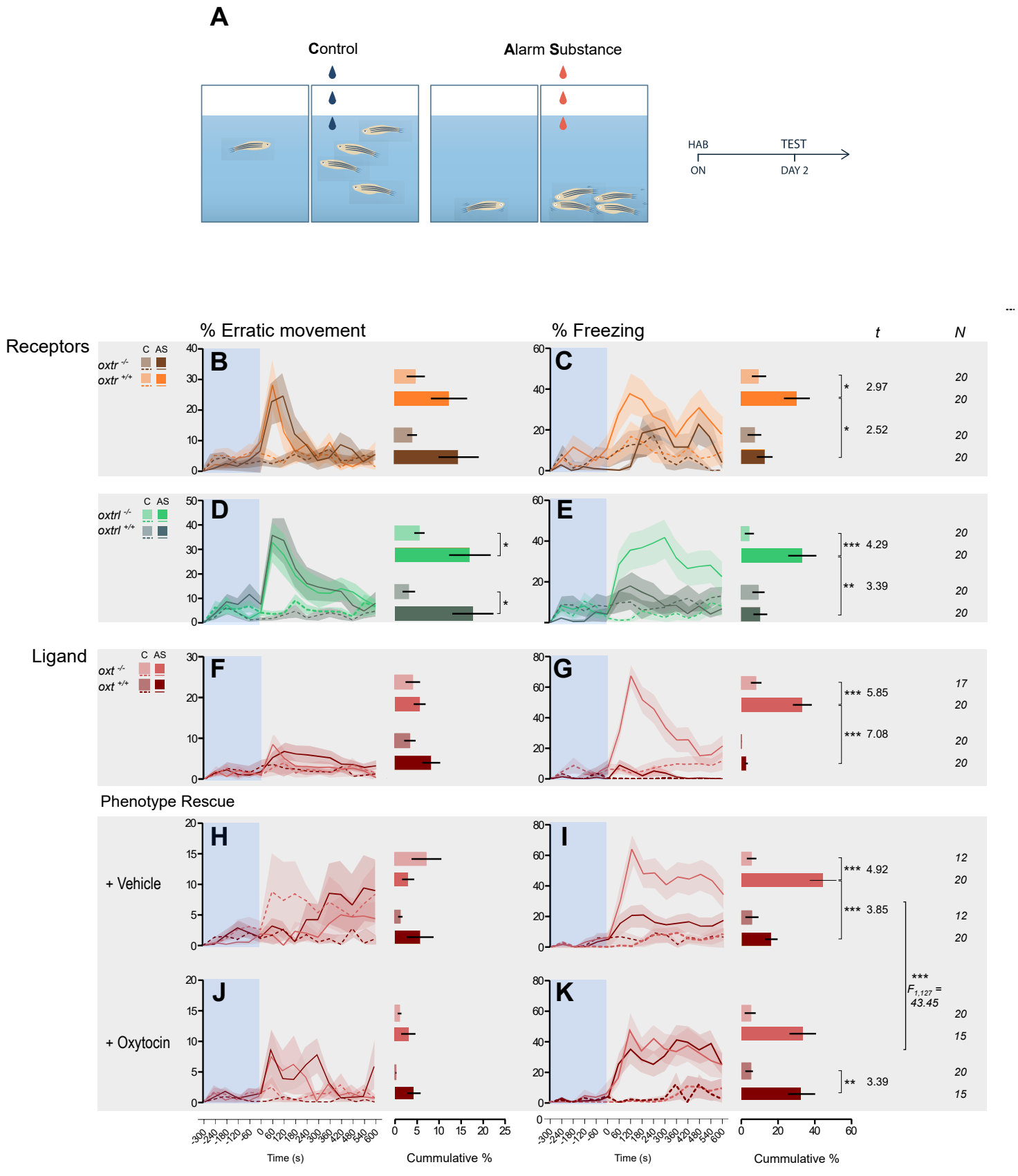

Fig 1. Oxytocin effects on the social transmission of distress. (**A**) Schematic and schedule (HAB, habituation; ON, overnight) of social contagion of fear paradigm. Droplets represent administration of vehicle (blue) and alarm substance (AS; red) to control and experimental groups. (**B-K**) Left panels: temporal dynamics of freezing and erratic movement response across treatments for mutant *oxtr*$^{(-/-)}$,*oxtrl*$^{(-/-)}$,*oxt*$^{(-/-)}$ and ligand rescue with intraperitoneal (i.p) oxytocin (OXT) to *oxt*$^{(-/-)}$ fish. Shaded area indicates time before AS or vehicle administration. Right panel: percentage of freezing and erratic movement (mean±SEM) after vehicle and AS administration. [*p < 0.05, **p < 0.01, ***p < 0.001]

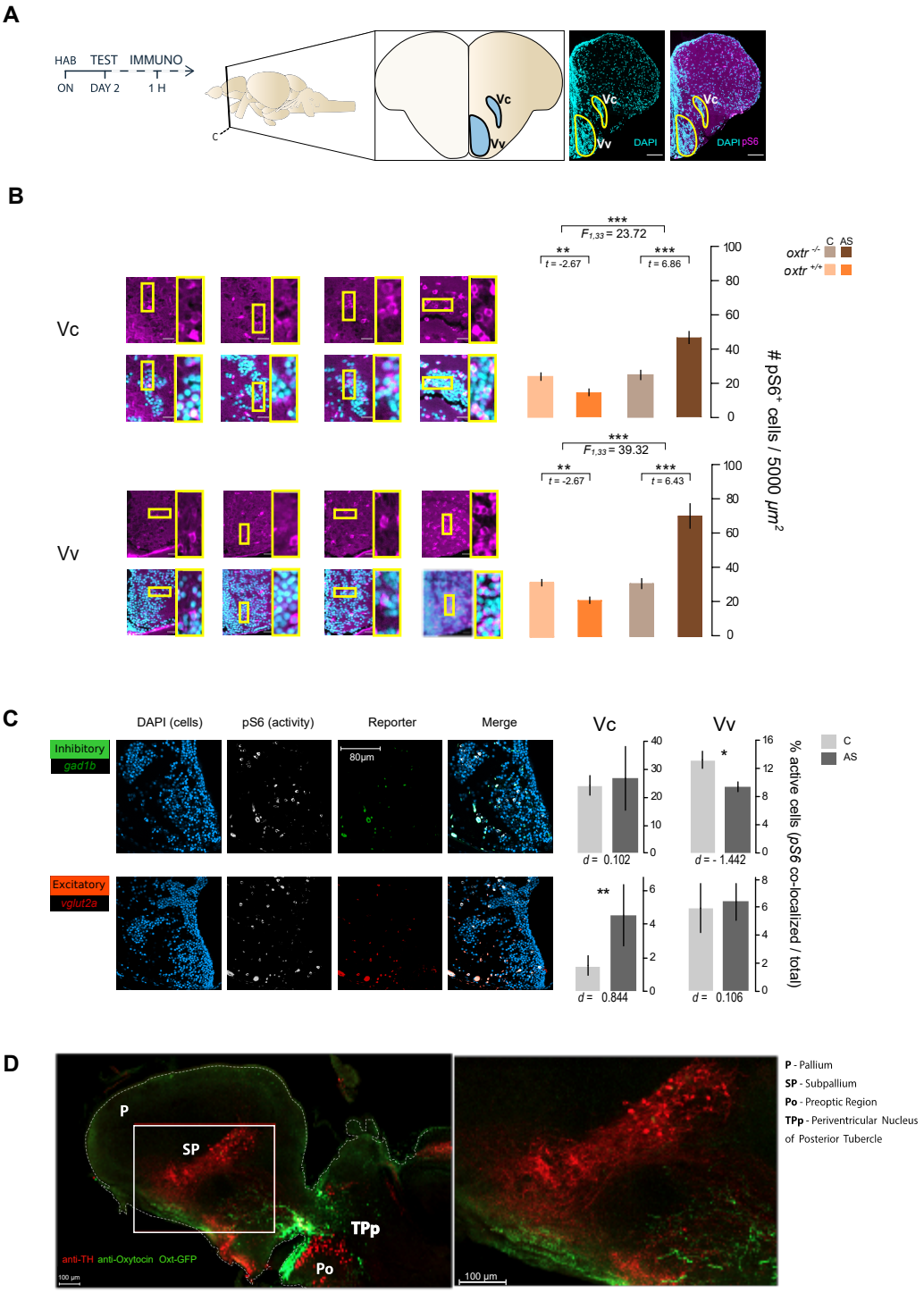

Fig 2. Oxytocin receptor deletion alters nodal neuronal activation. (**A**) Schedule of behavioural assay and immuno-staining; anatomical localization of the two brain areas responding to fear contagion: the ventral nucleus (Vv) and the central nucleus of the ventral telencephalon (Vc), with representative hemi-coronal sections identified by DAPI (cyan) and patterns of neuronal activity shown by pS6 (magenta) via immunostaining. (**B**) Quantification of the density (cells/5000 µm^2) of pS6 positive cells in each brain area (identified above the graph); panels show representative examples (left to right: wild-type control, wild-type alarm, mutant control, mutant alarm; scale = 20 µm). (**C**) Quantified activity in cells (pS6 and DAPI) identified as either excitatory (glutaminergic: *vglut2a*) or inhibitory (GABAergic: *gad1b*) in double reporter lines (*vglut2a:*dsRed / *gad1b:*GFP) compared between the observation of control or alarm-response in demonstrators (LMM, with pS6 as covariate; Cohen's *d* quantifies effect size), with representative microscopy examples shown in panels. [Results are shown as mean±SEM; *p < 0.05, **p < 0.01, *** p < 0.001]. (**D**) Representative example of sagittal brain slice (confocal maximum intensity z-stack) showing immunostained *oxt* positive neuronal fibers (green) projecting to the Vv in the subpallium of adult zebrafish with TH cell groups (red) also projecting to the Vv.

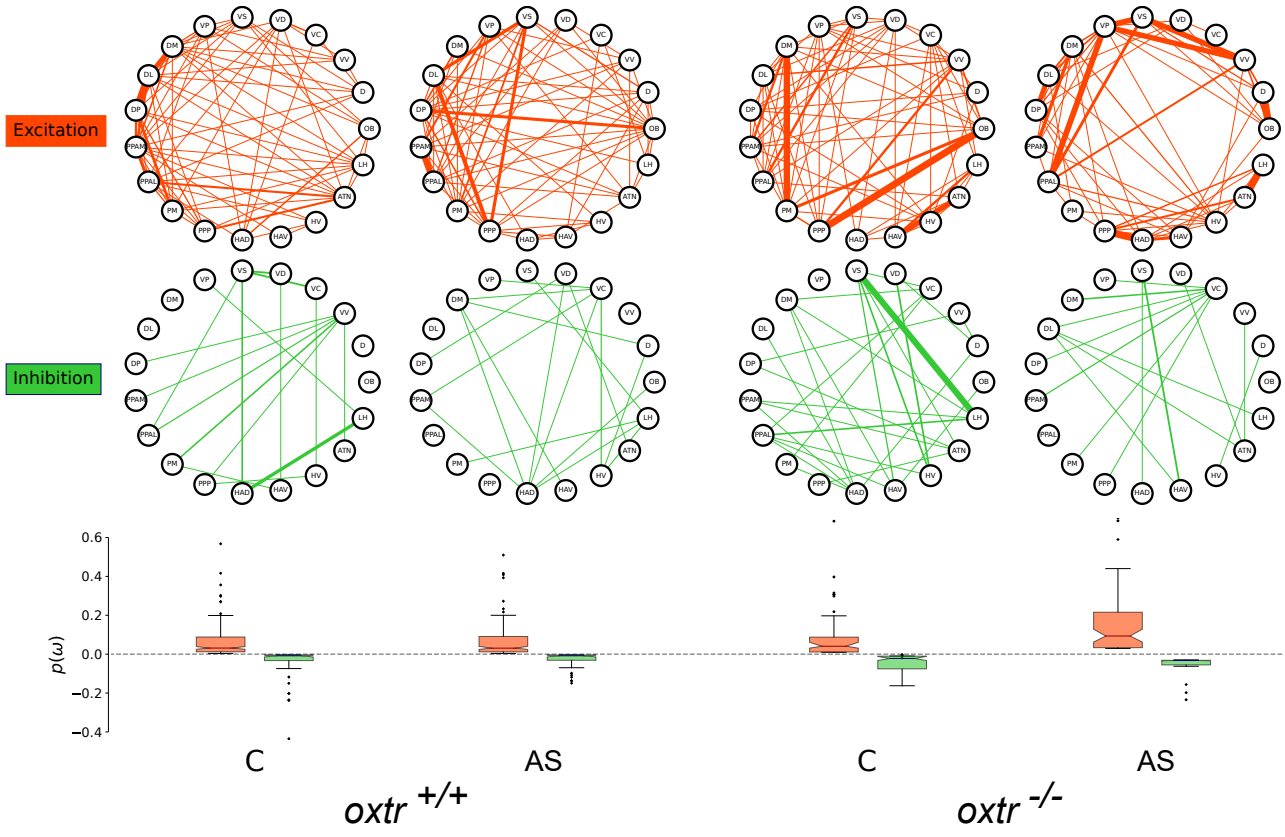

Fig 3. Network analysis of co-activation patterns in the social decision-making network. Nodes represent different regions and edges the relationship between them, where greater correlation values are represented by greater thickness. Networks were tested for both excitatory and inhibitory distributions across genotypes and treatments, and for computed average levels of each [probability in sample space, $p(\omega)$]. Under control conditions wild-types and mutants show differences in the network distribution (excitation: $KS = 0.23$, $p < 10^{-4}$; inhibition: $KS = 0.55$, $p < 10^{-6}$), but negligible differences in average signals (only inhibition: $U = 3492$, $p < 10^{-5}$, Cohen's $d = 0.18$). Under treatment, *oxtr* mutants exhibited both higher average excitation ($U = 5744$, $p < 10^{-6}$, Cohen's $d = 0.67$) and inhibition ($U = 1972$, $p < 10^{-6}$, Cohen's $d = 0.68$), as well as greater differences in distribution (excitation: $KS = 0.49$, $p<10^{-6}$; inhibition: $KS = 0.73$, $p<10^{-6}$).

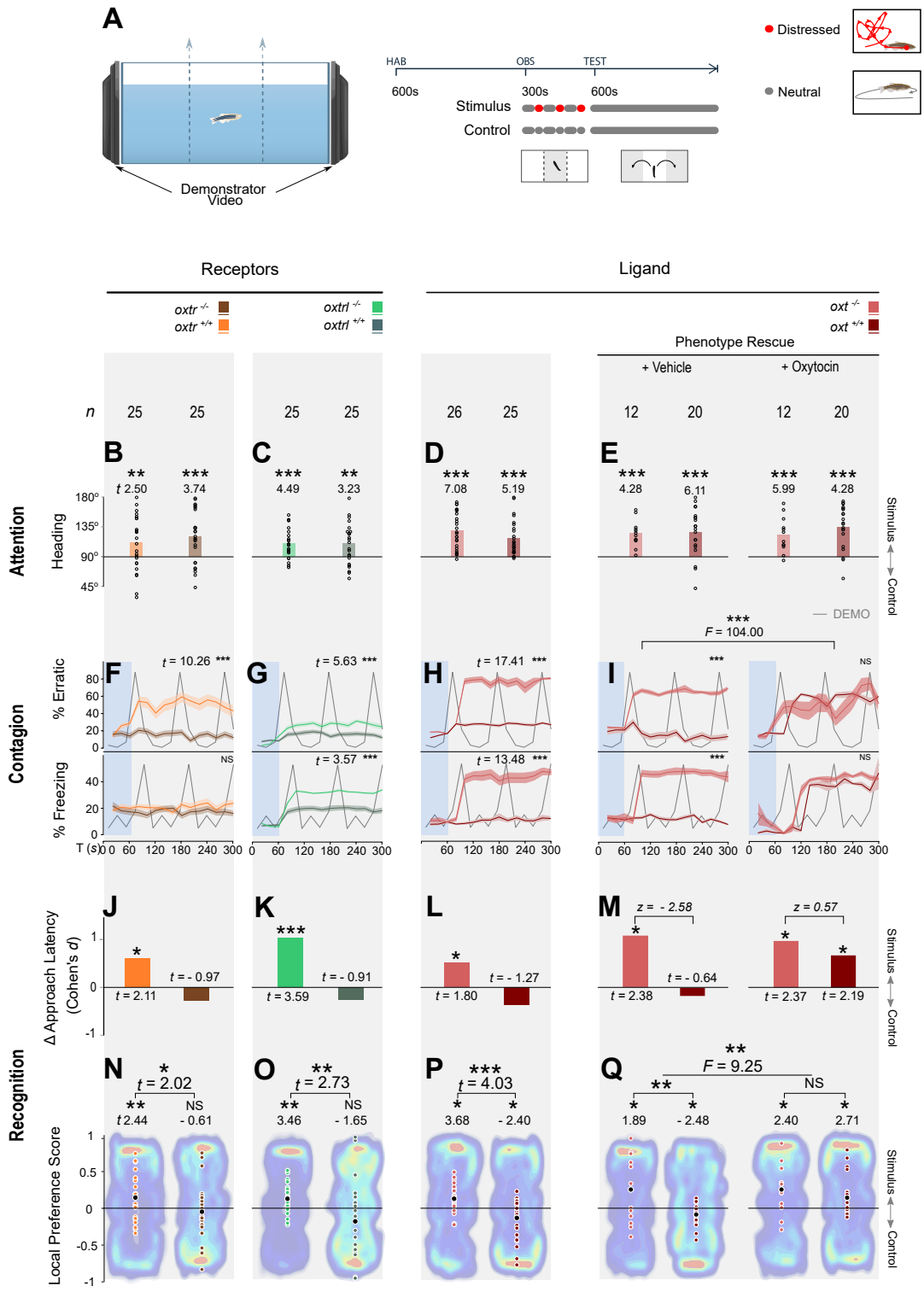

Fig. 4. Content validity of fear transmission by state recognition. (**A**) Video playback tests enabled the controlled assessment of stimulus versus state recognition across two experimental phases: a 5 min observation of two conflicting videos presenting the same demonstrator in either neutral state (control) or periodically distressed (stimulus); a 10 min local-preference test while both videos displayed the demonstrator in a neutral state. During observation, (**B-E**) attention was measured by the absolute heading towards the stimulus video (0 – 180 °; 1-sample *t*-tests, $\mu \neq 90°$) and (**F-H**) temporal changes in the proportion time erratic and freezing following analogous behavior in the stimulus video were compared between genotype and treatment (LMMs, full factorial). During tests, (**J-M**) differences in latency to first approach between the stimulus and control location were tested (Welch's 2-sample *t*-tests; effect-size comparisons: *z* tests, $d_1 \neq d_2$, $|z| \geq 1.96$ at $\alpha = 0.05$ two-sided) and (**N-Q**) local preference scores calculated based on cumulative durations (1-sample *t*-tests, $\mu \neq 0$; genotypic comparisons: Welch's 2-sample *t*-tests; genotype × treatment: two-way ANOVA with *post hoc* Fisher's LSD). Heat maps are representative examples with the least deviation from the mean. [$^{NS}P > 0.05$, $*P < 0.05$, $**P < 0.01$, $***P < 0.001$]

Supplementary materials for

Oxytocin regulation of social transmission of fear in zebrafish reveals its evolutionary conserved role in emotional contagion

Ibukun Akinrinade, Kyriacos Kareklas, Magda Teles, Thais K. Reis, Michael Gliksberg, Giovanni Petri, Gil Levkowitz, Rui F. Oliveira*

* corresponding author. E-mail: ruiol@ispa.pt

This PDF file includes:

Methods
Table S1
Figs. S1 to S5

Methods

Animals, housing and husbandry

We used naïve adult wild-type (WT) zebrafish, *Danio rerio,* of the *TU* strain (6-12 months) for characterizing the expression of oxytocin receptors. Transgenic reporter lines from a mixed *TL* background included *oxt*:EGFP for characterizing oxytocin fibre projections and double reporter *vglut2a:*dsred*/gad1b:*GFP for characterizing glutamatergic and GABAergic activity. In addition, we used WT and genetically modified (GM) adults from lines of a mixed *TL* background for testing the effects of oxytocin function on the social transmission of distress and the recognition of fear. All fish were housed in groups at a density of 10/L in a recirculation life support system (Tecniplast) maintained at 28 °C, pH 7.0, conductivity 1000 μS/cm and 14 L:10D photoperiod. Feeding included a combination of live (*Paramecium caudatum* and *Artemia salina)* and dry food (Gemma). Husbandry and health maintenance protocols were followed as previously described [31], and fish were kept free from known pathogens via sentinel testing. All experiments were conducted in accordance with standard operating procedures of the Institutional Ethics Committee, assessed and monitored by the Animal Welfare Body, and licensed by the National Competent Authority (DGAV-Direcção Geral de Alimentação e Veterinária, Portugal) with the permit number 0421/000/000/2020.

Genetic line characterization: modification of oxytocin signaling

The *oxt* mutant line (ZFIN ID: ZDB-ALT-180904-7) is a functionally null line with a small deletion of 7 base pairs in Exon 2 following treatment with CRISPR1-oxt at the

embryonic stage, described by Blechman et al. [32]. It is a frameshift mutation leading to disruption of the translational reading and abolishing the expression of the oxytocin neuropeptide, and thus overall oxytocin signaling. The *oxtr* mutant line (ZFIN ID: ZDB-ALT-190830–1) is a functionally null mutant line that has a small deletion of 1 base pair following treatment with TALEN1-oxtr at the embryonic stage. It is a frameshift mutation that abolishes the expression of oxytocin receptor 1. The characterization of the line has been further described by Nunes et al. [33]. The *oxtrl* transgenic line (ZFIN ID: ZDB-ALT-190819-1) has an insertion of a multi-frame stop cassette (83bp) at the ATG+260 position leading to a stop codon formation after the 89th amino acid, following CRISPR treatment at the embryonic stage, which abolishes the expression of the oxytocin receptor 2. Finally, the *oxt:EGFP* transgenic reporter line (ZFIN ID: ZDB-ALT-111103-1) was generated using the Tol2kit transposon-based vector system for encoding the *oxt* gene and report the endogenous expression of *oxt* mRNA and protein [32]. All genetic lines were generated at the Weizmann Institute of Science, Israel, by G. Levkowitz, and in collaboration with R. Nunes for the *oxtr* transgenic line and M. Gliksberg for the *oxtrl* line.

Genotyping

Genotyping was performed by PCR of the genomic region of interest from clipped fins, followed by sequencing [33]. We designed specific primer pairs to target the deletion sites of the ligand [*oxt* (NM_178291.2): 5` – AGACACAAACACTAAGTAA – 3` (forward), 5` – AGCAGACGGACAGCAGACACAGCA – 3` (reverse)] and receptors [*oxtr* (NM_001199370.1): 5‘ – TGCGCGAGGAAAACTAGTT – 3‘ (forward), 5‘ – AGCAGACACTCAGAATGGTCA – 3‘ (reverse); *oxtrl* (NM_001199369.1): 5‘ – TTTTACGCACAATGGAGAGCC – 3‘ (forward), 5` – AGCATGTAAGTGGACGCGAA – 3’ (reverse)].

Alarm substance extraction

Alarm substance was extracted by following approved procedures under institutional and project licenses. Briefly, 12 adult fish of either sex (to control for variations) were euthanised via rapid chilling, placed on a petri dish kept on ice and 15 superficial surgical-blade cuts were performed on either side of their trunk to induce the release of alarm substance from the club cells. Cuts were then washed with 50ml of distilled water and filtered with a 240mm filter paper (VWR cat no. 516-0287) to remove impurities. The extracted solution from all fish was mixed and stored in individual aliquots of 0.75 ml in -20^{o}C.

Oxytocin treatment

To test the reversal of effects from non-functioning oxytocin signalling, *oxt* KO and WT controls were treated with either the fish homologue of oxytocin (isotocin; *Ser4*, *Ile8*-Oxytocin; Cat. No. 4030890.0005, Bachem, Germany) or vehicle controls. For the treatment, first were anaesthetised by immersion in MS-222 solution (100mg/L), weighted and placed with their ventral part exposed in a pre-cut fissure on a spongy bed saturated in water. Fish

were then administered a 2 µl/g (μ weight = 2.5g ± 0.8) intraperitoneal injection (30G needle) of either saline (vehicle control) or isotocin solution in saline (0.9%) at 1ng/kg, based on dose-response tests by Braida et al. [34]. The administration period was ~20s, after which fish were placed in a small compartment with tank water and allowed 2 min to recover with the help of oxygen supply from air bubbles slowly pipetted near their gills.

Behavioral test for social transmission of fear

Focal fish were randomly assigned to either of three conditions: to observe a shoal exposed to the alarm substance, to observe a shoal exposed to distilled water (vehicle control) or to be exposed to the alarm substance directly without observing any demonstrators (control for social transmission). The order of testing was randomized for each individual and conducted between 10:00 and 19:00. Animals were removed from home tanks on the day before experiments, randomly assigned to treatment groups, and kept in their experimental tank overnight for acclimatization. Experimental tanks had visual access to identical adjacent tanks (1.3 L; 12 × 12 × 15 cm), but were visually isolated from other external cues via opaque covers. Adjacent tanks kept either a shoal of two males and two females (Fig. 1A), or remained empty for the social transmission control. Each trial lasted for 15 min, including a 5 min baseline period followed by a 10 min post-exposure period. The alarm substance was kept on ice to avoid degradation during the trials and, thus, distilled water for the vehicle control was kept in the same conditions. Substances were administered via a flexible and transparent PVC tubing (diameter: 0.8 mm internal, 2.4 mm external).

Behavioral test of fear recognition

This test used video playbacks, which enabled us to control for inter-individual variation in demonstrators by presenting focal fish videos of the same fish in two separate states, neutral and fearful. The ability of fish to perceive and respond to videos of conspecifics under identical conditions, was demonstrated by Nunes et al. [33], which provide a detailed analysis of response to features of biological motion. Demonstrators used in video playbacks were recorded with a goPro camera (goPro hero3+, 60 fps, 1080 pixel resolution) placed in front of a 1.5 L tank, behind an opaque acrylic sheet with a customised cut-out for the camera lens, in order to keep the investigator covered during manipulations. The rest of the tank walls kept covered to reduce further visual interference and contained a flexible and transparent PVC tubing for substance administration (diameter: 0.8 mm internal, 2.4 mm external). A 10 minute recording of the tank was first captured to be used during the acclimatisation phase of experiments. Each fish used as a demonstrator was kept in the tank overnight, with the camera in place, and the following morning was recorded. During recording, following a 200s capture of baseline behaviour, the investigator released 0.75 ml (per 1.3L of water) of alarm substance and recorded for a further 200s, to capture erratic movement and freezing behaviour. Videos were edited using the VSDC© software (v. 6.3.6.18; Flash-Integro LLC, 2019) and included: a 10 min video of the housing tank of demonstrators used as *background video* during acclimation (Fig. S); a 5 min *control video* with the demonstrator swimming (neutral state), which included 3 repetitions of a 100s swimming period (Video S1); a 5 min *stimulus video*

with the demonstrator periodically exhibiting fear, which included 3 repetitions of a 60s swimming period followed by 40s bout of an erratic and freezing repertoire (Video S2). During tests, videos were displayed on monitors as real size images.

Experiments were carried out in a 4.5 L test tank (29.5 × 14.5 × 11 cm), stationed on a light box with infrared LEDs and with two LCD monitors (Asus VG248, 1080 HD, 144 Hz rapid refresh rate) positioned on either side, remaining visible through the glass walls **(**Fig. 4A**)**. The rest of the tank was covered with opaque lining and the overall set-up was housed in a compartment covered with a light-blocking black fabric to prevent visual interference from external stimuli. Playback screens were controlled and synchronised via a third screen connected to the same computer (TightVNC remote control software). Focal fish were kept in overnight isolation, housed individually in opaque tanks (12 × 12 × 15 cm) at 28 °C and a 14 L: 10 D photoperiod. The following day fish were individually placed in a central compartment of the test tank, devised by two removable transparent partitions, and acclimatized for 10m to the background video projected by both LCD screens. Following acclimation, one monitor was set to play the 5 min control video (neutral state) and the other the stimulus video (periodic fearful state), with the side of the video and the identity of the demonstrator (1 male and 1 female) counterbalanced across subjects. Following this stage, the partitions were lifted and fish allowed access to the entire tank for 10 min while playbacks on both sides displayed the control video (played twice in sequence).

Data extraction

For each test a continuous video-recording was obtained, using a high definition camera for the fear transmission test (Logitech B 525; acquisition at 30 fps) and a black-and-white camera with infrared sensitivity (Henelec 300B; acquisition at 30 fps) for the fear recognition test. The shift to the infra-red recording in the second test facilitated automated tracking over the larger arena, using the infra-red light backdrop from experimental set-up (Fig. 4A). Videos were fed to a remote laptop computer using the recording software Pinnacle Studio (v. 12, http://www.pinnaclesys.com). Individual recordings were then analyzed using the commercially available video tracking software Ethovision XT© 11.0 (Noldus Inc., The Netherlands).

For the fear transmission tests, recordings of the whole tank were tracked over the 15 min trial period in order to extract measures used to quantify fear behavior, both for the 5 min baseline period and the 10 min post-exposure period. These included proportion time spent exhibiting erratic movement [acceleration > 8 cm/s^2 and > 5 changes in direction/sec (> 90°)] and freezing (velocity < 0.2 cm/s).

For the fear recognition tests two separate stages were scored. First, for the first 5 min period of video observation, the zone of the central compartment in which animals were restricted was set as a region of interest (ROI) and animals tracked within this region. Attention to video playbacks was measured by the absolute compass heading (*x* direction relative to the stimulus video, ranging from 0° to 180°). Fear transmission was again measured by proportion

time in erratic movement and freezing, and validated by added kinematic quantifiers [angular velocity (turn angle per frame); speed (cm/s)], and matched to the same measures extracted from the playback videos for validating transmission. Second, for the final 10 min of the test, during which full-tank access was allowed, the compartments next to each video were set as ROIs (Fig. 4A) and 3 measures were extracted: total distance travelled (exploration); latency time to first entry at either ROI (approach motivation); and the total time spend within each ROI (local preference).

Quantification of neuronal activation using the neuronal activation marker phospho-S6 ribosomal protein (pS6)

Brain tissue was collected for the quantification of brain activation and functional connectivity in *oxtr* experimental fish (mutants and WT controls) following the social transmission of fear experiment (1 hr post testing). Animals were anaesthetized with ice-cold water and their head extracted by cervical transection, fixed in 10% formalin for 3 days (in room temperature; RT), rinsed twice in 1× PBS (30min) and kept in EDTA (0.5 M, pH=8) for a further 2 days (RT). Coronal sections (5µm) of samples were extracted for immunohistochemical staining and microscopy, following paraffin-embedding.

Sectioned brains were stained for the pS6. Slides were first kept in Tris-EDTA at 95°C (20 min) for antigen retrieval. Non-specific binding was blocked by a 1 hr in 1% BSA TBS incubation (0.025% Triton X-100) at RT and an overnight incubation in the primary antibody prepared in blocking solution (pS6 $Ser^{235/236}$ antibody D57.2.2E Rabbit mAB #4858 1:400; at 4 °C. Slides were then rinsed in TBS (0.025% Triton X-100) and incubated in the secondary antibody prepared in blocking solution (Alexa 594- Invitrogen goat anti-rabbit # A-11037 1:1000, Alexa 488- Invitrogen goat anti-chicken A-11039 1:1000). Slides were then washed in TBS with and then without 0.025% Triton X-100, before 20 min incubation in DAPI (4',6-diamidino-2-phenylindole) for nuclei counterstaining and rinsed in TBS before mounting (Biotium, Everbrite- 23003).

pS6 positive cells quantification projections visualization was performed on 20-fold magnified sections (Zeiss Axioscan.Z1 slide scanner) and analyzed via the Zeiss Zen blue 2.1 imaging software. Five consecutive coronal sections were quantified for each brain region (Fig. S5), where positive pS6 cells were counted in 1000 µm quadrants.

Quantification of active inhibitory (GABA) and excitatory (glutamte) cells

To quantify excitatory and inhibitory activity in experimental fish of the double reporter line *vglut2a:*dsred / *gad1b:*GFP, following the social transmission of fear experiment (1 hr post testing), we used immunostaining with pS6 and DAPI to identify active cells, and with GFP and dsRed antibodies to quantify GABA (*gad1b*) and glutamate (*vglut2a*) sites, respectively.

On day one of the immunostaining protocol, slides were deparaffinized and exposed to antigen with Tris-EDTA (10mM TrisBase, 1mMEDTA) 0.05% Tween 20, pH 9.0. Samples were then incubated in Tris-EDTA at 95°C for 20 min, removed and left to chill without the

lid for 15 min, washed three times in TBS 0.025% Triton X-100 with gentle shaking for 10 min, and blocked by incubation with TBS 0.025% Triton X-100 + 1% BSA (albumin) for 1 hr at room temperature. The samples were finally incubated with the primary antibody [anti-pS6 (mouse; 1:400), anti-GFP (chicken; 1:200), anti-dsRed (rabbit; 1:200)] in TBS 0.025% Triton X-100 + 1% BSA overnight at 4°C in humid chamber.

On day two, samples were first washed in TBS 0.025% Triton X-100 (3 times for10min) by gentle shaking and incubated with the secondary antibody (1:500; anti-mouse 647, anti-chicken 488, anti-rabbit 568) in TBS 0.025% Triton X-100 + 1% BSA for 2 hr at room temperature. Samples were then washed in TBS 0.025 Triton X-100 (twice for 10 min) by gentle shaking and finally incubated in DAPI (1:500 in TBS) for 20 min at room temperature, before mounting slices with EverBrite Hardset medium.

Stained brain sections were acquired at 20-fold magification using the Zeiss Imager Z2 + ApoTome.2 slide scanner and analyzed using the ImageJ Java software. Slices were counted alternately so that cells were not considered in duplicate. In each region, we identified DAPI stained cells with the pS6 signal and counted the total as well as those overlapping with either the GFP (GABA; *gad1b*) or dsRed (glutamate; *vglut2a*) signals. Co-localizations of pS6 positive cells with either GFP or dsRed were measured in % active cells such that:

$$\%\ \text{active} = \left(\frac{no.\ colocalized\ with\ pS6}{total\ no.}\right) \times 100$$

Imaging of oxytocin projections

OXT:GFP (Tg(*oxt*:EGFP)wz01 ID: ZDB-ALT-111103–1) positive fish were sacrificed in Tricaine, and their heads and skull removed. the heads were then fixed O.N at 4C in 4% PFA on a shaker. After fixation the brains were removed from the skull and subjected to whole-mount immunohistochemistry as per standard protocol: PFA was washed out, and samples were placed in ice cold (-20C) acetone in a freezer at -20C for 10 minutes. The acetone was washed out, and the samples were then incubated in blocking solution (PBS + 0.1% triton, 1% DMSO, 1% BSA, 5% NGS) for minimum of 2 hours at R.T and then incubated with primary Ab diluted at 1:200 ((anti-TH, Mouse monoclonal anti-Tyrosine hydroxylase, Merck-millipore, CAT: #MAB318) and anti-GFP (Chicken polyclonal anti-GFP IgY Antibody Fraction, Life Technologies, CAT: #A10262)) O.N at 4C on the shaker. The following morning, Samples were washed repeatedly (minimum of 6X15 minute washes) with blocking solution and then placed in blocking solution containing fluorescent secondary antibody at 1:200 O.N at 4C on a shaker. The following morning, Brains were submerged in 4% Noble Agarose, allowed to cool at 4C, and then sliced in a vibratome in ice-cold PBS at a thickness of 200 um. Slices were then mounted on a slide in mounting medium (Aqua-Polymount, polysciences, inc. 400 valley road, Warrington PA 18976, CAT: 18606-20) and imaged on a Zeis LSM 800 scanning confocal microscope.

Expression of oxytocin receptors in the brain

Brain tissue was also collected for testing the expression of oxytocin receptors (oxtr and oxtrl) in WT fish. WT fish samples were embedded in cryomoulds (OCT Compound, Tissue-Tek, Sakura 4583) and cryosectioned (150 µm coronal, Leica CM 3050S cryostat) for microdissection.

Receptor expression in WT fish was tested following microdissection of target brain areas from the cryosections, collected under stereoscope (Zeiss Stemi 2000) with a modified 210 µm needle (1 per region to prevent cross-contamination). Target areas were selected based on their involvement in social regulation and decision making [15] and included: the olfactory bulb (Ob), the medial zone of the dorsal telencephalic area (Dm, putative homologue of the mammalian basolateral amygdala), the preoptic area (POA), and the ventral nucleus of the ventral telencephalic area (Vv, putative homologue of the mammalian lateral septum), the dorsal nucleus of the ventral telencephalic area (Vd, putative homologue of the mammalian striatum), the supracommissural nucleus of the ventral telencephalic area (Vs, putative homologue of the mammalian medial extended amygdala and the bed nucleus of the stria terminalis), and the postcommissural nucleus of ventral telencephalic area (Vp). The Ob, Vv, Vd, Vs/Vp (pooled due to proximity), and POA were collected from both hemispheres at a single sampling point, due to their small size when compared to the diameter of the microdissection. The Dm was sampled from both hemispheres separately, and tissue was then pooled directly into lysis buffer and stored at -80°C until mRNA extraction.

For RNA extraction tissue was homogenized in 100 μl of qiazol (lysis buffer) and incubated for 7 min at RT. 50 μl of Chloroform was then added and shaken vigorously for 15 s and the sample left to incubate at RT for 5 min. Samples were then centrifuged at 13000 g for 20 min at 4ºC, and the upper aqueous phase transferred to a new tube where 1 volume of 70% ethanol was added. This mixture was transferred to an RNEasy® column and left to stand for 5 min at RT, and then was centrifuged for 1 min at 9000 g. A series of buffers from the RNeasy® Lipid Tissue Mini Kit (Qiagen, 74804) were added to samples sequentially (700 μl of Buffer RW1, 500 μl of Buffer RPE and an additional 500 μl Buffer RPE), after each of which samples were centrifuged for 1 min at 9000 g and the flow-through discarded. The RNeasy column was then centrifuged a new 2 ml tube for 3 min at 14000 g and transferred to a separate new 1.5 ml tube where RNA was eluted with 25 μl of RNAse-free water, and centrifuged for 2 min at 9000 g. The elution step was repeated with the same RNAse-free water to increase RNA recovery efficiency and RNA screened for concentration, purity (260 nm and 280nm spectrophotometric absorbance; Thermo Scientific NanoDrop 2000) and integrity (Agilent 2100 Bioanalyzer).

Pooled RNA of each brain area was reverse transcribed to cDNA (iScript cDNA Synthesis Kit, Biorad, 1708890) following the manufacturer's instructions. Briefly, in a clean Eppendorf tube, nuclease-free water, 5x iScript reaction mix (4μl), iScript reverse transcriptase (1μl), and RNA template (100 fg to 1 μg total RNA) were added up to a total volume of 20 μl and incubated in a PCR thermocycler (5 min priming at 25°C, 60 min reverse transcription at 42°C, 5 mins reverse transcription inactivation at 85°C, and kept at 4°C). Samples were subsequently stored in -20°C until use.

Diluted cDNA samples (1:10) were used as templates for quantitative polymerase chain reactions (qRT-PCR). Primer sequences for the oxytocin receptor (*oxtr*) and the reference gene (*eef1a1l1*: eukaryotic translation elongation factor 1 alpha 1, like 1) were designed in the Primer 3 software (Premier Biosoft International, Palo Alto, CA, USA) and primer sequences for oxytocin receptor-like (*oxtrl*) were provided by Gil Levkowitz. qRT-PCR reactions were performed in the Applied Biosystems quantstudio 7 thermocycler (7900 HT, Thermofisher) in 8 *µl* triplicate reactions with SYBR Green PCR Master Mix (Applied Biosystems, Thermofisher) with 50 µM primers for *oxtr* and *eef1a*, and 13.3 µM for *oxtrl*. Thermocycling conditions were 5 min at 95°C, followed by 40 cycles of 95°C for 30 s, annealing temperature 60°C for 30 s, and extension at 72°C for 30 s. After PCR, a melting curve program from 55 to 95°C with 0.5°C changes was applied and fluorescence cycle thresholds (*Ct*) were automatically measured.

Analysis

Statistical analyses, calculations and graphical representations were carried out using the software Graphpad Prism® (v. 8.0.1; GraphPad LLC, San Diego, CA), R© (v. 4.0.3; R Core Team) and Minitab® (v.17; Minitab Inc., State College, PA). Figures were edited and completed with illustrations using the software Adobe® Illustrator® (CS6, v.16.0.0; Adobe Systems Inc.) and Inkscape© (v. 0.92.4; Free Software Foundation Inc.). Continuous data were tested for normality using the Ryan-Joiner and Kolmogorov-Smirnov tests and homogeneity of variance was tested using the Bonnett's and Levene's tests. Finite ranging and proportion based scores were tested for normality using the D'Agostino & Pearson test (K^2), which confirms Gaussian distribution via skewness and kurtosis [35].

Genetic expression of receptor genes was calculated using the $2^{-\Delta Ct}$ method [36]:

$$2^{-\Delta Ct} = 2^{Ct_{Ref} - Ct_{Target}}$$

where Ct_{Ref} is the cycle threshold for the reference gene and Ct_{Target} is the cycle threshold for the target gene. Therefore, target gene expression was represented as relatively to the reference gene and quantified by the mean of this value across three technical replicates.

Cell counts of pS6 positive cells were tested via a generalized linear model with quasi-Poisson regression, with treatment (alarm substance or control) and genotype as fixed factors. A backward stepwise procedure was used to exclude non-significant effects, followed by *post-hoc* comparisons corrected with the two-stage linear step-up procedure for FDR-adjusted p-values.

Counts of GFP and dsRed positive sites with pS6 positive cells were tested via a generalized linear regression model with a log-link function, with treatment (alarm substance or control) as

a fixed factor, and the total number of pS6 positive cells as a random covariate to control for individual differences from overall activity.

Percentage time erratic and freezing were compared between treatment groups using unpaired *t*-tests for parametric data, Welch's 2-sample *t*-tests for non-homogeneous normal data, and Mann-Whitney *U* tests for non-parametric data. Comparisons between lines were carried out using ANOVA tests, either at the two-way with treatment (alarm or control), or at the three-way when examining added effects from oxytocin injection (versus control) for testing recovery. Data not conforming to parametric assumptions were log-transformed [$log_{10}(x + 1)$]. *Post-hoc* comparisons for testing differences between the treatments were corrected with False Discovery Rate (FDR) and *p*-value adjusted (Benjamini and Hochberg's method).

Compass orientation (absolute heading in degrees) was tested for differences from 90˚ by 1-sample *t*-tests to compare deviations from divided attention (see Fig. 2A) and compared between groups using Welch's 2-sample *t*-tests (due to unequal sample sizes).

Angular velocity and speed for each individual was measure by mean values from across the 3 replicates during observation, for both the 40s stress demonstration period and separately for the immediately preceding 40s under control conditions (neutral, swimming), in 10s time bins. For each of the two periods, stress and neutral control demonstration, we calculated the total area under the curve (AUC) across time bins using the trapezoid approximation method:

$$AUC_{t_{1-t_2}} = \frac{(x_1+x_2)}{2} \times (t_1 - t_2)$$

Behavioural change between states was then calculated as the difference in AUC between the control and stress demonstration periods (Δ AUC), for both speed and angular velocity. These values of change were tested for significant deviation from no difference ($\mu \neq 0$) by 1-sample *t*-tests and compared between groups using Welch's 2-sample *t*-tests (due to unequal sample sizes). To examine the degree of stress contagion, we tested consistency between observer and demonstrator angular velocity and speed using a linear regression model with time bin as an interaction term for time-dependent changes.

Total distance travelled (cm) was compared between genotypes for all lines by Welch's 2-sample *t*-tests. To test for the effect of injections we used a two-way ANOVA with treatment (oxytocin or vehicle injection) and its interaction with genotype (WT or *oxt* KO) as predictors, and *post hoc* comparisons using Fisher's LSD.

Approach latency (s) towards the stimulus video ROI, where the demonstrator periodically stressed during observation, was compared to the approach latency towards the control-video ROI by Welch's 2-sample *t*-tests on the mean (due to unequal sample sizes) and effect sizes calculated using Cohen's *d* and the proportion of mean change, for each group. To assess the reversal of effects following injection treatments, for both the oxytocin and the vehicle treatment, we compared the directional effect size between WT and *oxt* KO. To do this we first calculated the sampling variance of each group:

$$v = \frac{1}{n_1} + \frac{1}{n_2} + \frac{d^2}{2(n_1 + n_2)}$$

and used this to compare Cohen's *d* values between genotypes, using a *z*-test:

$$z = \frac{d_1 - d_2}{\sqrt{v_1 - v_2}}$$

where for normal distributions the null hypothesis ($H_0 : d_1 = d_2$) can be rejected if $|z| \geq 1.96$ at $\alpha = 0.05$ (two-sided).

Preference scores (PS) were calculated based on the time spend in ROI near the stimulus (ROI_S) and the control video (ROI_C) using:

$$PS = \frac{(ROI_S - ROI_C)}{(ROI_S + ROI_C)}$$

where values range between -1 (full preference for control) and 1 (full preference for stimulus). In order to validate that preference levels were statistically different from chance, we first tested if mean preference scores for each group were significantly greater or lower than 0, depending on the direction, by using 1-sample *t*-tests. Comparisons of preference scores between WT and KO fish for each line were performed using Welch's 2-sample *t*-tests (due to unequal sample sizes). To test for the effect of injections we used a two-way ANOVA with treatment (oxytocin or vehicle injection) and its interaction with genotype as predictors, and *post hoc* comparisons using Fisher's LSD.

For brain connectivity analysis, networks representing the co-activation patterns for each treatment were constructed as follows. For the case of M specimens, characterized by one sample (cell count) reading x_i for each of the N brain regions, the M-dimensional vector $\mathbf{x}_i$ was considered, where *i* labels the region, and then computes the correlations c_{ij} for all region pairs, obtaining a weighted correlation matrix that we interpret as the adjacency matrix of a functional network. We then filtered each layer using the networks for each treatment as described by De Vico Fallani et al. [37] keeping the links with larger weight (in absolute value) up to a threshold density of $\rho = 0.17$. For the analysis of the excitation and inhibition patterns, we separate the weighted and signed graph in two subgraphs containing respectively only the positive and negative links, which we interpret as pertaining to network excitation and inhibition configurations. Distributions were compared by the two-sample Kolmogorov-Smirnov test and averages using the Mann-Whitney *U* test.

For the ranking of node strengths and correlations we compared, for all treatments, the strength (weighted degree of the full correlation matrix) of nodes in the standard way and rank them in descending order. To assess, similarities between ranking corresponding to different treatments, Kendall-Tau rank correlations were used and only correlations with $p<0.01$ were retained as significantly different from zero.

For the Detection of communities and extraction of conserved submodules we used the spin glass community detection method [38] applied on the average treatment network, obtained by averaging over the corresponding graph tower matrices. To increase the robustness of the detection, for each treatment, we repeated the community detection 1000 times. We computed the (center) consensus partition for each treatment from the 1000 candidate partitions, extracted as described by Peixoto [39].

To identify parts of modules that are shared between communities in different treatments, we study the distribution of intersection sizes. In particular, for two partitions we consider partitions $P_y = \{C_y^0, C_x^1, \ldots . C_x^m\}$ and $P_y = \{C_y^0, C_y^1, \ldots . C_y^l\}$ for treatments x and y, and then compare for each pair of modules (C_x^i, C_y^j) the intersection $J_{x,y}^{i,j} = C_x^i \cap C_y^j$ and then measure its cardinality$|J_{x,y}^{i,j}|$. We compute the significance of the measured intersection sizes by a permutation test based on a null distribution $p_0(|J|)$ constructed as follows: for a pair (C_x^i, C_y^j), we sample uniformly at random 10000 pairs of node sets with cardinality respectively $|C_x^i|$ and $|C_y^j|$and compute the size $|J|$ of their intersection. We consider statistically significant and thus retain the observed submodules $J_{x,y}^{i,j}$ such that $|J_{x,y}^{i,j}| > \mu(|J|) + 3\sigma(|J|)$ (equivalent to a p < 0.01 significance threshold), where $\mu(|J|)$ and $\sigma(|J|)$ are the first two moments of $p_0(|J|)$.

References

31. Borges, A. C., Pereira, N., Franco, M., Vale, L., Pereira, M., Cunha, M. V., ... & Rebelo, M. (2016). Implementation of a zebrafish health program in a research facility: A 4-year retrospective study. *Zebrafish*, *13*(S1), S-115

32. Blechman, J., Anbalagan, S., Matthews, G. G., & Levkowitz, G. (2018). Genome editing reveals idiosyncrasy of CNGA2 ion channel-directed antibody immunoreactivity toward oxytocin. *Frontiers in Cell and Developmental Biology*, *6*, 117.

33. Nunes, A. R., Carreira, L., Anbalagan, S., Blechman, J., Levkowitz, G., & Oliveira, R. F. (2020). Perceptual mechanisms of social affiliation in zebrafish. *Scientific reports*, *10*(1), 1-14.

34. Braida, D., Donzelli, A., Martucci, R., Capurro, V., Busnelli, M., Chini, B., & Sala, M. (2012). Neurohypophyseal hormones manipulation modulate social and anxiety-related behavior in zebrafish. *Psychopharmacology*, *220*(2), 319-330.

35. D'Agostino, R. B. (1986) Tests for Normal Distribution. In: *Goodness-Of-Fit Techniques* (ed. D'Agostino RB and Stephens MA) 68, Macel Dekker

36. Livak, K. J., & Schmittgen, T. D. (2001). Analysis of relative gene expression data using real-time quantitative PCR and the 2− ΔΔCT method. *Methods*, *25*(4), 402-408.

37. De Vico Fallani, F., Latora, V., & Chavez, M. (2017). A topological criterion for filtering information in complex brain networks. *PLoS computational biology*, *13*(1), e1005305.)

38. Traag, V. A., & Bruggeman, J. (2009). Community detection in networks with positive and negative links. *Physical Review E*, *80*(3), 036115.

39. Peixoto, T. P. (2021). Revealing consensus and dissensus between network partitions. *Physical Review X*, *11*(2), 021003.

Table S1. Ranks of node strengths for each treatment for both wild-types and mutants.

	Wild-types		**Mutants**	
	Control	**Alarm**	**Control**	**Alarm**
0	DL	PPP	PM	VP
1	DP	VS	OB	VV
2	PPAM	PPAL	PPP	PPAL
3	DM	DL	DM	VS
4	PPAL	PPAM	HAV	PPP
5	ATN	DP	VV	HAD
6	PPP	OB	ATN	D
7	PM	VP	PPAM	OB
8	OB	VV	DL	ATN
9	VP	PM	DP	LH
10	D	D	VP	DM
11	VD	HAV	PPAL	DP
12	LH	ATN	VC	DL
13	VC	DM	D	HV
14	HV	VD	HV	PPAM
15	HAV	VC	HAD	HAV
16	VS	LH	VD	VD
17	VV	HAD	LH	PM

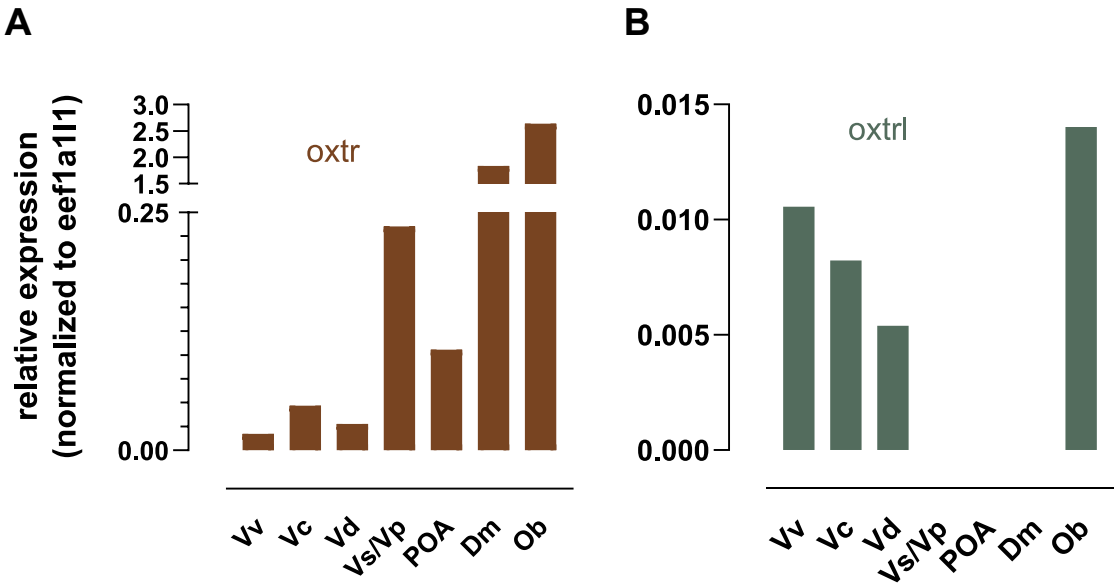

Fig. S1. Relative expression of the two oxytocin receptors in areas of the social decision-making network in the zebrafish forebrain. (**A**) The main receptor (*oxtr*) was expressed in all areas of the network and in greater levels than (**B**) the second receptor (*oxtrl*), which was limited in the olfactory bulb (Ob) and the central, ventral and dorsal nucleus of the ventral telencephalon (Vc, Vv, Vd).

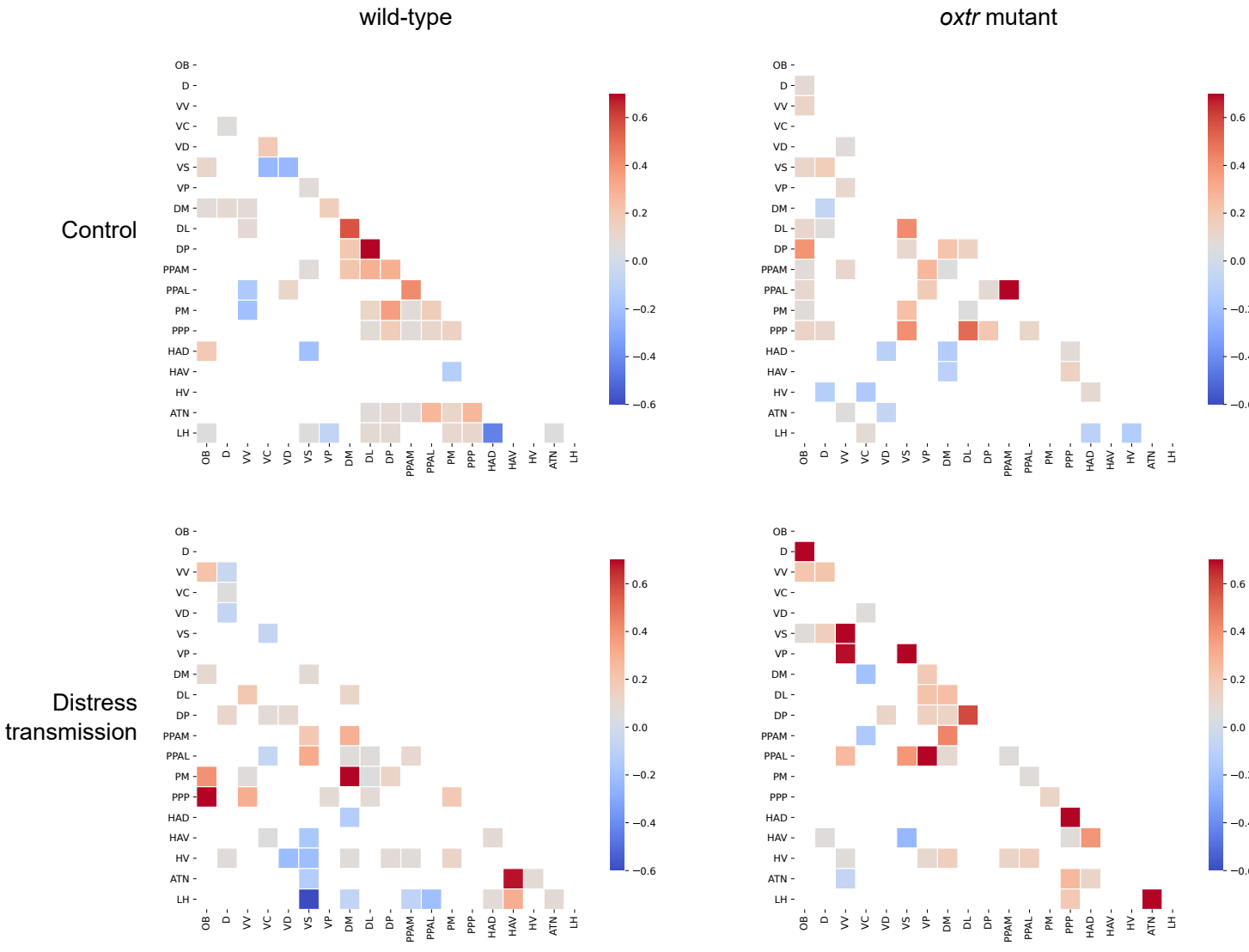

Fig. S2. Adjacency matrices indicating inter-area connectivity. Each area's (node's) linkage with all other nodes (spearman's correlations) indicate it's centrality, which shifted with condition and genotype.

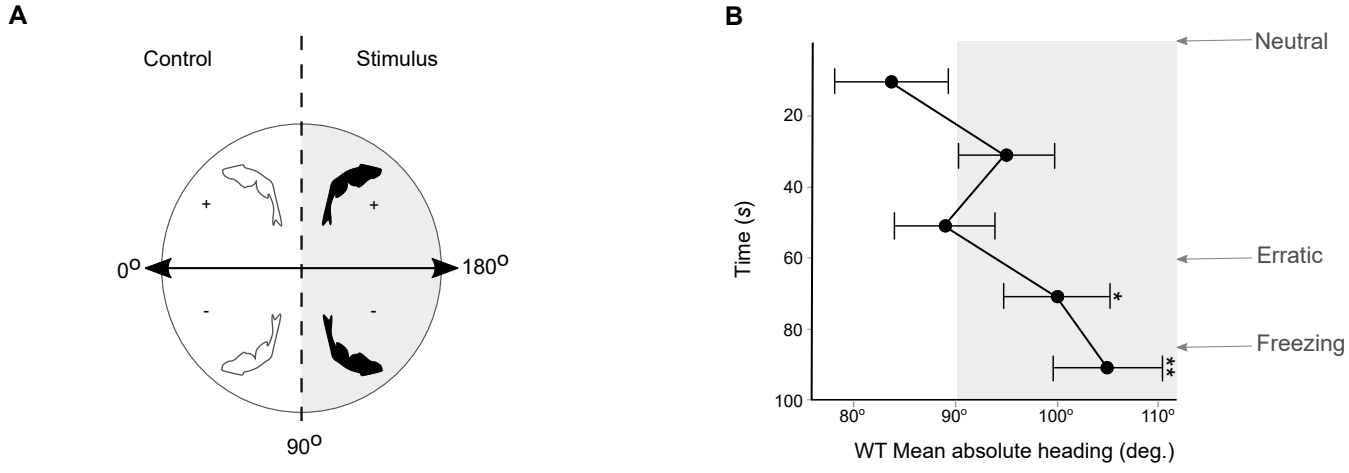

Fig. S3. Quantification of attention towards observed neutral (control) and distress state (stimulus). (**A**) Absolute heading towards (0 - 180 degrees) the stimulus was used to measure distress-elicited shifts in attention. (**B**) Changes in attention over observation time indicate that divided attention undersimultatnesous presentations of neutral behaviour ($\mu > 90^{O}$; $p > 0.05$) shifts away from neutral behaviour and towards both erratic ($t_{25} = 1.91$, $p = 0.03$) and freezing ($t_{25} = 2.83$, $p = 0.003$) behaviour when distress is demonstrated by the stimulus.

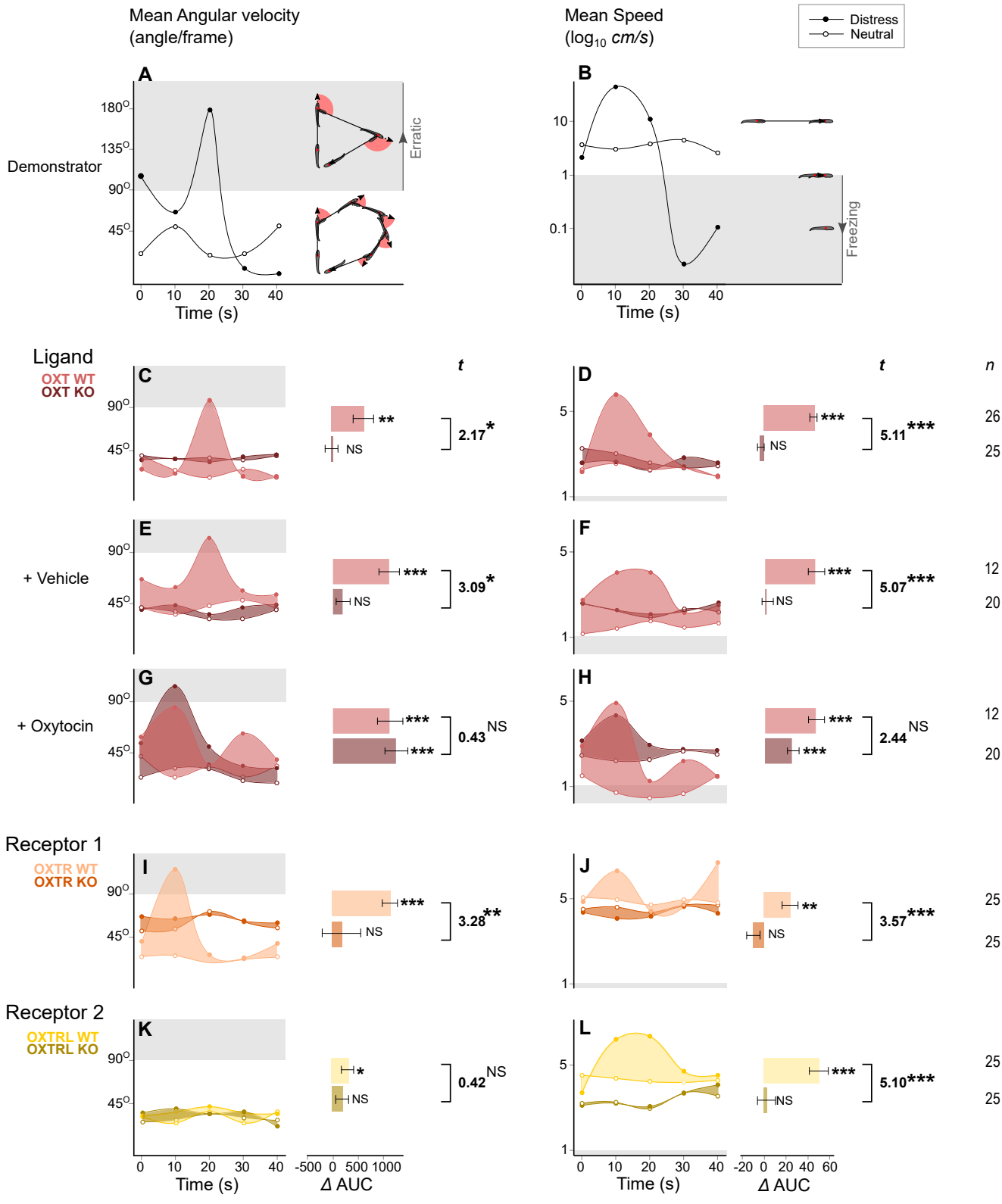

Fig. S4. Immediate response to stress state changes. Changes from neutral to distressed behavior by the demonstrator led to: (**A**) increases in angular velocity with erratic movement ; (**B**) decreases in speed during freezing. (**C**) Angular velocity and (**D**) speed changes with demonstrator shifts between neutral and stress behavior were exhibited in WT but not *oxt* KO observers. (**E, F**) Genotypic effects under control treatments (vehicle), contrasted (**G, H**) KO fish phenotype recovery by oxytocin treatment. (**I**) Angular velocity increases implicated the expression of the first receptor (*oxtr*). (**J**) Speed changes were exhibited by WT, but not *oxtr* KO observers. (**K**) Expression of the second receptor (*oxtrl*) led to increases in angular velocity, but without significant differences between WT and KO observers. (**L**) Speed changes were significantly influenced by *oxtrl* expression. Degree changes are indicated by difference in the area under the curve (*Δ* AUC) from neutral to stress state observations. [per-group: 1-sample *t*-tests, $\mu \neq 0$; between-groups: Welch's *t*-tests; $^{NS}P > 0.05$ *$P < 0.05$, **$P < 0.01$, ***$P < 0.001$]

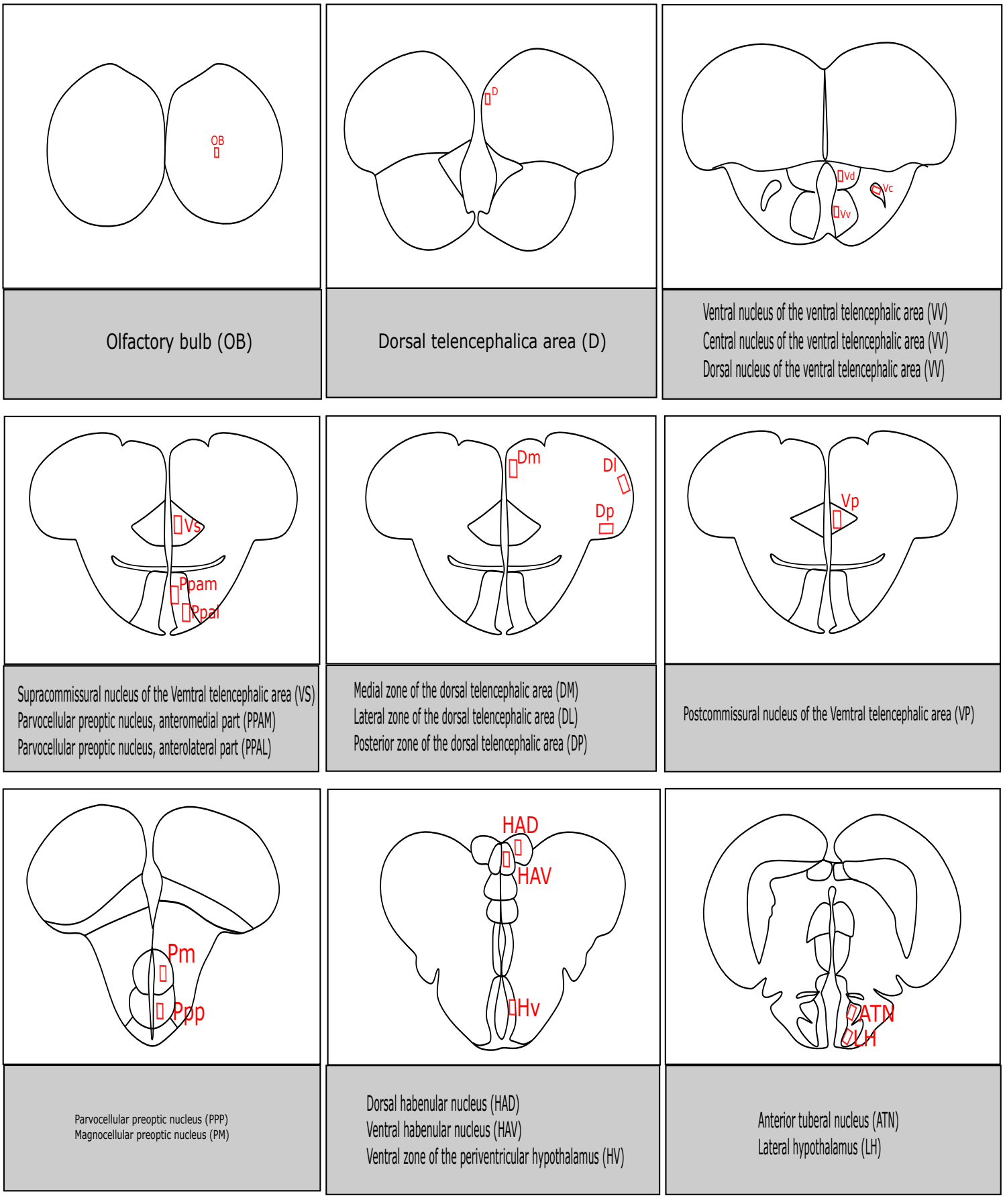

Fig. S5. Identification of brain regions involved in social buffering of fear. The social decision-making network; a combination of the social behaviour network and the reward system (O'Connell & Hofmann, 2011). Red rectangles represent brain regions of interest for quantifying pS6 positive cells; brain regions of interest were identified using the zebrafish atlas (Wullimann MF, Rupp B and Reichert Vogel, 1996).